Europium "Second Generation" Precursors for Metal-Organic Chemical Vapor Deposition: Characterization and Optical Spectroscopy

Graziella Malandrino,*[a] Marco Bettinelli,*[b] Adolfo Speghini,[b] and Ignazio Luciano Fragalà[a]

Keywords: Luminescence / Chemical vapor deposition / Europium / Polyether adducts

The novel complex precursor $Eu(hfa)_3$·monoglyme and the analogous $Eu(hfa)_3$·diglyme [Hhfa = 1,1,1,5,5,5-hexafluoroacetylacetone, monoglyme = $CH_3OCH_2CH_2OCH_3$, diglyme = $CH_3O(CH_2CH_2O)_2CH_3$] have been synthesized in a single step reaction and characterized by elemental analysis, mass spectrometry, and IR and Raman spectroscopy. Thermogravimetric data and the linear evaporation behavior have shown that both complexes are thermally stable and can be evaporated to leave less than 4% residue. Luminescence spectra in the visible region provided evidence of a remarkable covalent character of the metal-ligand bonding in both complexes with the distortion of the coordination sphere around the europium(III) ion in $Eu(hfa)_3$·monoglyme greater than that in $Eu(hfa)_3$·diglyme. DSC measurements and variable temperature luminescence spectra have shown the presence of a structural transition at 71.4 °C from a solid to a plastic phase for $Eu(hfa)_3$·diglyme.

Introduction

Several efforts have recently been devoted to the design of novel lanthanide complexes with suitable mass transport properties for metal-organic chemical vapor deposition (MOCVD) applications.[1−4] This is due to the severe drawbacks of first generation MOCVD precursor complexes, i.e. their thermal instability, reactivity with oxygen, low volatility, and high residues left upon sublimation. In addition, their use as precursors for MOCVD deposition of LnF_3 and LnOF requires the use of an additional fluorine source.[5]

Conversely, the polyether adducts of lanthanide fluorinated β-diketonates[6−14] exhibit improved properties in terms of thermal stability and volatility, thus representing a class of novel second-generation precursors that has been successfully applied to the MOCVD fabrication of various materials.[7,8,14−17] These adducts represent single-source precursors for the MOCVD fabrication of LnF_3 and LnOF (Ln = La, Gd) phases[7,8,17] which are challenging host matrices for different applications such as X-ray storage phosphors, laser materials, and optical waveguides.

In this context, MOCVD techniques offer several advantages[18] over classical physical techniques and are well suited for depositing good quality films even for those applications where high performances are required as, for example, the deposition of epitaxial Pr-doped BaF_2 on a CaF_2 substrate for optical waveguide applications.[19]

Herein, we report the synthesis, physicochemical characterization, and mass transport properties of the novel europium MOCVD precursor $Eu(hfa)_3$·monoglyme [Hhfa = 1,1,1,5,5,5-hexafluoroacetylacetone, monoglyme = $CH_3OCH_2CH_2OCH_3$]. We also report a viable and safer route (than that already proposed[20]) to the analogue $Eu(hfa)_3$·diglyme [diglyme = $CH_3O(CH_2CH_2O)_2CH_3$]. The europium(III) ion has been chosen among the trivalent lanthanide ions due to its intense luminescence in the visible region that opens up several opportunities for technological applications and represents an important tool to study both the coordination geometry and the coupling with the surrounding vibrations.[21] In addition, the laser-excited and vibrational Raman spectroscopy of these adducts are discussed and compared with the Gd analogues.[7]

Results and Discussion

Synthesis

The $Eu(hfa)_3$·L adducts have been prepared through a one-pot reaction from europium oxide, hexafluoroacetylacetone and the polyether in hexane [Equation (1)]:

$$1/2Eu_2O_3 + 3Hhfa + L \rightarrow Eu(hfa)_3\cdot L + 3/2H_2O \quad (1)$$

The slight excess of europium oxide favors the isolation of the product since the insoluble unreacted Eu_2O_3 may be easily filtered off. In contrast with the previously reported procedures for the analogous lanthanum precursors[6] as well as for $Eu(hfa)_3$·diglyme,[20] the present methodology avoids the use of carcinogenic benzene. It is worth noting that the present $Eu(hfa)_3$·monoglyme adduct, at variance with the $La(hfa)_3$·monoglyme·H_2O homologue, is water-free. This is clearly due to the smaller ionic radius of the europium(III) ion, which enables the monoglyme ligand to saturate the coordination sphere, thus preventing any water coordination.

[a] Dipartimento di Scienze Chimiche, Università di Catania, Viale A. Doria 6, 95125 Catania, Italy
[b] Dipartimento Scientifico e Tecnologico, Università di Verona, Ca' Vignal, Strada Le Grazie 15, 37134 Verona, Italy

 © WILEY-VCH Verlag GmbH, 69451 Weinheim, 2001 1434−1948/01/0404−1039 $ 17.50+.50/0

The present adducts are very soluble in common organic solvents such as ethanol, chloroform, acetone, pentane, toluene and slightly soluble in cyclohexane. Both adducts have low melting points and sublime quantitatively at low temperature under vacuum. They are nonhygroscopic and can be handled in air.

Infrared Spectra

The IR spectra of the crude and sublimed $Eu(hfa)_3$·polyether adducts show identical features. The absence of any bands around 3600 cm^{-1} in the spectra of **1** and **2** is indicative of H_2O-free species. All the spectra show singular absorption bands around 1650 cm^{-1}, due to C=O stretching vibrations, and at 1520 cm^{-1}, due to the C=C stretching vibrations. The other bands, observed at 1100−1300 cm^{-1}, represent C−O bending and/or stretching of the polyether ligand overlapping with the C−F stretching frequencies. Peaks around 860 and 1050 cm^{-1} are indicative of glyme coordination to the europium hexafluoroacetylacetonate moiety.[8]

Raman Spectra

The room temperature vibrational Raman spectra of pelletized powders of **1** and **2** and of the corresponding gadolinium analogues are virtually identical for wavenumbers lower than 1500 cm^{-1}. As a representative example, we show in Figure 1 the Raman spectrum of **2**.

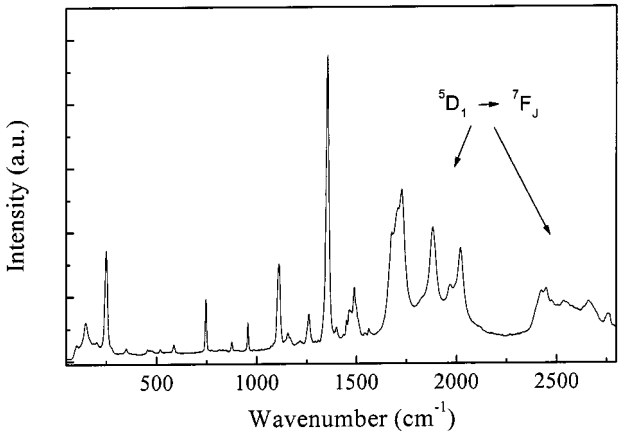

Figure 1. Room temperature Raman spectrum of **2** (λ_{EXC} = 488.0 nm)

The prominent peak at about 1350 cm^{-1} is assigned to vibrations involving the -CF_3 grouping, whilst the bands close to 1500 cm^{-1} are assigned to modes involving -CH_2- deformations.[22] The sharp peak at 250 cm^{-1} is due to a metal-oxygen vibration.[23] In the case of the spectra of the europium(III) compounds **1** and **2**, additional peaks are present in the 1500−3000 cm^{-1} spectral region which are missing in the corresponding spectra of the gadolinium analogues. These features are assigned to electronic emission transitions from the $^5D_1$ excited state to the ^7F_J ground multiplet of europium(III), as they are not observed in the Raman spectrum of the isostructural gadolinium complex, and on the basis of the energy level structure of europium(III) ion, as already observed for different hosts.[24]

Thermogravimetric and Calorimetric Data

The thermal behavior of the raw adducts **1** and **2** has been studied by thermal gravimetric analysis (TG), and differential scanning calorimetry (DSC) under N_2. The TG curves of **1** and **2** show singular sublimation steps (Figure 2) in the 100−246 °C (residue = 3% to 290 °C) and 113−255 °C (residue = 2% to 260 °C) temperature ranges, respectively.

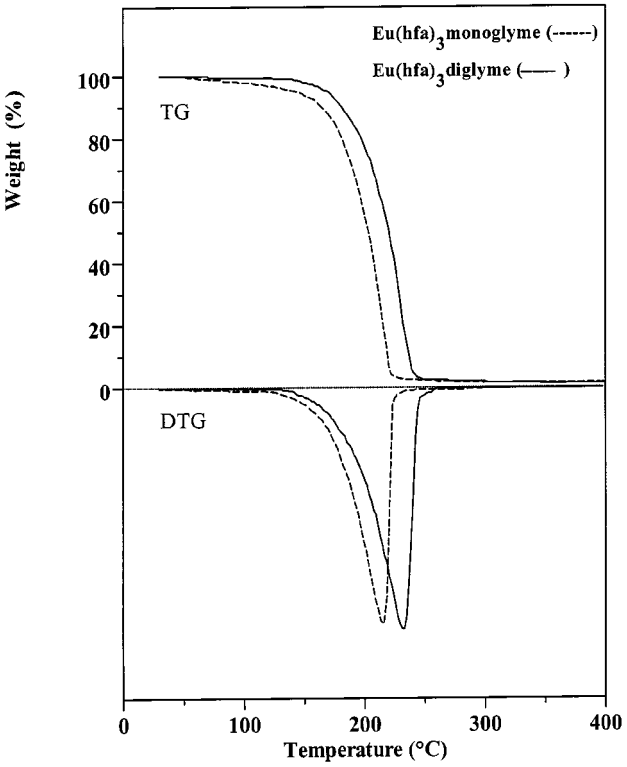

Figure 2. TG-DTG curves of adducts **1** and **2**

The linear behavior of the TG atmospheric pressure vaporization rates (Figure 3) of adducts **1** and **2** indicate that both adducts are thermally stable and, therefore, represent interesting precursors for MOCVD applications.

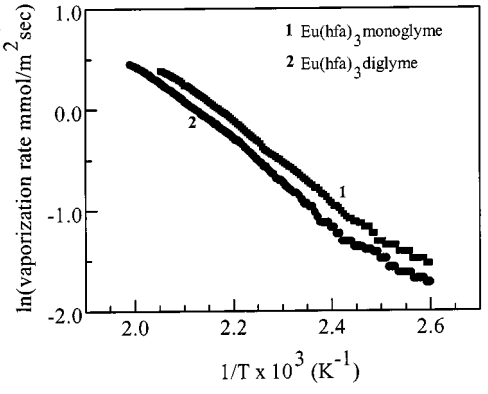

Figure 3. DSC curves of adducts **1** and **2**

The DSC curves of $Eu(hfa)_3$·L adducts are reported in Figure 4. Adduct **1** shows a sharp melting point at 81.2 °C (9.14 cal/g), in good agreement with that observed with a Koffler Microscope (80−82 °C). Evaporation from the melt occurs afterwards. The DSC curve of the diglyme adduct **2** shows some interesting features. Two sharp endothermic peaks are observed at 71.4 °C (9.26 cal/g) and 122.0 °C (1.04 cal/g). Several consecutive heating and cooling DSC experiments in the 30−150 °C temperature range have shown the disappearance of the first peak after the first cycle. The second peak, in contrast, remains unchanged in terms of both the temperature and the ΔH associated with the process. The peak at 71.4 °C again becomes evident after standing for several hours at room temperature. This endothermic process represents a "thermal anomaly"[25] and may be associated with a transition from the solid to a plastic phase.[9] The second peak is associated with the complete melting. This conclusion agrees well with the optical microscopy observations upon heating, which show the disappearance of the crystal color at 73−76 °C and complete melting at 123−126 °C.

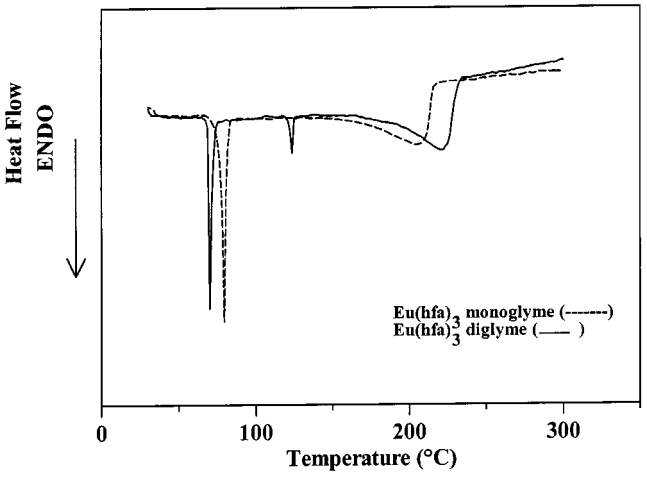

Figure 4. Atmospheric pressure TG vaporization rate data of adducts **1** and **2** as a function of the temperature

Finally, it is interesting to remark that the DSC features of **1** and **2** are almost identical to those of the Gd homologues. Note that both the Eu[20] and Gd[7] diglyme adducts, in fact, have identical crystal structures within the same space group and almost identical unit-cell dimensions (0.01 Å difference between corresponding cell parameters).

Mass Spectra

The FAB spectra of adducts **1** and **2** show peaks due to the loss of both the hfa ligand and the polyether (see Table 1).

Peaks arising from the characteristic fluorine transfer process, already found in the spectra of the alkaline earth[26] and analogous lanthanide[7,8] β-diketonate polyether adducts, are also observed. The observed MS peaks are associated with $[Eu(hfa)_2$·polyether$]^+$, $[Eu(hfa)$·polyether + $F]^+$, $[Eu(hfa)_2]^+$, $[Eu(hfa) + F]^+$, $[Eu$·polyether + $2F]^+$ and $[EuF_2]^+$ fragments. No molecular ion peaks or peaks at higher mass have been observed, in agreement with the monomeric nature of the complexes.

Table 1. Major peaks in the mass spectra of adducts **1** and **2**; the given *m*/*z* ratios are related to the isotope ^{153}Eu

Assignment	$Eu(hfa)_3$·monoglyme	$Eu(hfa)_3$·diglyme
$[Eu(hfa)_2$·L$]^+$	657 (100%)	701 (100%)
$[Eu(hfa)$·L + F$]^+$	469 (28%)	513 (19%)
$[Eu(hfa)$·L$]^+$	450 (15%)	494 (36%)
$[Eu(hfa)$ + F$]^+$	379 (11%)	379 (<5%)
$[Eu(hfa)]^+$	360 (75%)	360 (21%)
$[Eu$·L + 2F$]^+$	281 (12%)	325 (11%)
$[Eu$·L + F$]^+$	262 (<5%)	306 (9%)

Luminescence Spectra

The room-temperature, laser-excited luminescence spectra of powders of **1** and **2**, measured with an excitation wavelength of 488.0 nm, consist of $f \rightarrow f$ emission transitions from the $^5D_0$ excited state to the ^7F_J multiplet of the europium(III) ion. The $^5D_0 \rightarrow {}^7F_0$ transition cannot be split by the crystal field and its profile gives information on the number of different coordination sites accommodating the europium(III) ion. The presence of a single band in the high resolution luminescence spectra of both **1** and **2** indicates that the europium(III) ion occupies a single site in both compounds. In the case of **2**, this observation agrees well with the X-ray single-crystal structure reported by Kang et al.,[20] in which only one europium(III) site is present, as well as with the crystal structure of the isostructural gadolinium(III) compound.[7]

The peak position of the $^5D_0 \rightarrow {}^7F_0$ transition is related to the nephelauxetic effect and to the covalency of the europium(III)−ligand bond.[27] In both **1** and **2** the $^5D_0 \rightarrow {}^7F_0$ maxima are located in the "covalent" region of the nephelauxetic scale,[27,28] but in the case of **1** the $^5D_0 \rightarrow {}^7F_0$ peak occurs at a longer wavelength than in **2** (see Table 2). This is indicative of a greater europium(III)-ligand covalency in the former.

The ratio of the integrated intensities of the $^5D_0 \rightarrow {}^7F_2$ and $^5D_0 \rightarrow {}^7F_1$ transitions [Equation (2)] can be considered indicative of the asymmetry of the coordination polyhedron of the europium(III) ion[29] and can thus be used to compare the degree of distortion in complexes having similar ligand arrays. The rather high R value (6.6) of **2** points to a distorted first coordination sphere around the europium(III) ion (point symmetry C_1), as found in the crystal structure determination.[20] In the case of **1**, whose crystal structure is not known, the even higher R value (11.0) is indication of a very asymmetric europium(III) site.

$$R = \frac{I(^5D_0 \rightarrow {}^7F_2)}{I(^5D_0 \rightarrow {}^7F_1)}$$

The overall crystal field (CF) splitting values associated with the $^7F_1$ state are reported in Table 2. The smaller crystal field splitting observed in **1** can be correlated to a smaller (than in **2**) europium(III) coordination number. In fact, the crystal data of $Eu(hfa)_3$·diglyme[20] point to a coor-

Table 2. Measured intensity ratios R, peak luminescence wavelengths λ_{max} of the $^5D_0 \rightarrow {}^7F_0$ transition, crystal field splittings of the $^7F_1$ state and lifetimes τ of the $^5D_0$ excited state of europium(III) for the two compounds under investigation

Compound	R	$\lambda_{max}(^5D_0 \rightarrow {}^7F_0)$/nm	CF splitting ($^7F_1$)/cm^{-1}	$\tau(^5D_0)$/ms
Eu(hfa)$_3$·monoglyme	11.0	579.9	251	0.93
Eu(hfa)$_3$·diglyme	6.6	579.4	292	0.96

dination number of nine for the europium(III) ion, while an eight-coordinate environment can be assumed for **1**, with both hfa and monoglyme acting as bidentate ligands, since no water molecules are coordinated to the metal ion.

The luminescence excitation spectra of both **1** and **2**, associated with the $^5D_0 \rightarrow {}^7F_2$ transition, consist of sharp $f \rightarrow f$ transitions for wavelengths higher than 450 nm, and of a broad band peaking at about 400 nm (Figure 5). The latter feature is assigned to an Eu−O ligand-to-metal charge transfer transition[30] since both polyether and hfa ligands do not show absorption bands in this spectral region.

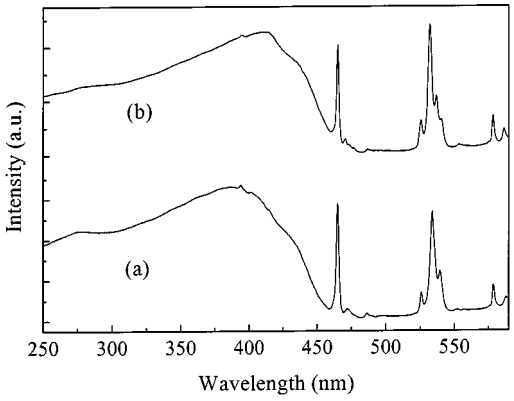

Figure 5. Room temperature excitation spectra of adducts **1** (a) and **2** (b)

Inspection of the high resolution, room-temperature luminescence spectrum (Figure 6) shows that a weak structure is located in both the high- and low-energy sides of the $^5D_0 \rightarrow {}^7F_0$ pure electronic transition. These features are assigned to vibronic sidebands due to coupling between the $^5D_0 \rightarrow {}^7F_0$ electronic transition and the vibrational modes involving the europium(III) ion.[31,32] Vibronic sidebands have often been observed in the luminescence and excitation spectra of europium(III)-doped crystalline and noncrystalline solids.[33,34] Less frequently they have also been observed in the spectra of europium(III) coordination compounds.[35] In general, vibronic sidebands mainly relative to the $^5D_0 \rightleftarrows {}^7F_2$ transition have usually been studied.[36]

The maxima in the vibronic sideband at lower energy are located about 80, 150 and 250 cm^{-1} from the pure electronic line in the case of **1,** and 80, 140, 185 and 250 cm^{-1} in the case of **2**. These differences are assigned to the wavenumbers of vibrational modes coupled to the europium(III) electronic transitions and, therefore, localized close to the metal ion. The vibrations are assigned to Eu−O modes, due to their small wavenumber values. In particular, the maximum at 250 cm^{-1} agrees with the presently proposed assignment of the Raman band at the same frequency to the

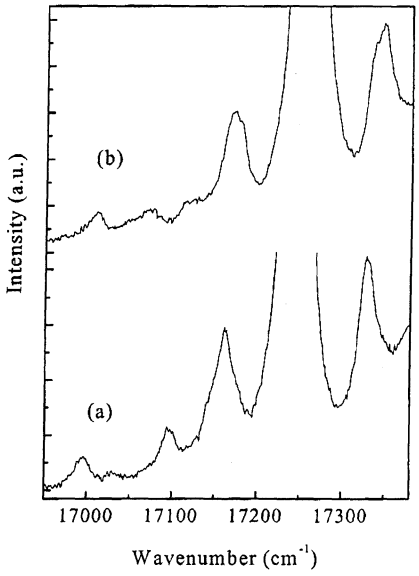

Figure 6. Room temperature luminescence spectra of adducts **1** (a) and **2** (b)

Eu−O stretching mode (vide supra). The other modes observed in the vibronic sideband probably represent other stretching and bending modes at the europium(III) center.

The luminescence decay curves from the europium(III) $^5D_0$ state in **1** and **2**, measured at room temperature, with excitation and observation wavelengths of 395.0 and 613.0 nm, respectively, are perfectly exponential for about three decades. The associated lifetimes of the $^5D_0$ state [$\tau(^5D_0)$, Table 2] are relatively short for europium(III) compounds (<1 ms), but compatible with both the high intensity of the hypersensitive $^5D_0 \rightarrow {}^7F_2$ emission transition and the presence of high frequency vibrations in the complexes. The exponential decays, in addition, are indicative that energy transfer and migration processes are probably inefficient in these compounds due to the rather long distance [8.047 Å in the gadolinium(III) homologue of **2**][37] between neighboring metal centers in the crystals.

The nature of the "thermal anomaly" observed at 71.4 °C in the DSC curves of **2** has been also investigated by low resolution luminescence spectra in the temperature range 20−90 °C. The experimental data show that the spectra do not change significantly for temperatures up to about 80 °C. Beyond this temperature, the intensities of the $^5D_0 \rightarrow {}^7F_2$ and $^5D_0 \rightarrow {}^7F_0$ emission transitions increase abruptly, compared to the magnetic dipole $^5D_0 \rightarrow {}^7F_1$ transition, so that the asymmetry ratio *R* approaches the value of 12 at 90° C. This clearly indicates that beyond 80 °C the first coordination sphere of the europium(III) ion undergoes a marked distortion, possibly due to the transition to a plastic phase.

We note that the *R* value associated with **2** in the plastic phase lies close to that found for **1** in the solid phase. Therefore, it is possible that packing constraints force the coordination geometry of europium(III) in the solid phase of **2** to be more symmetrical than in the plastic phase.

MOCVD Depositions

Preliminary MOCVD experiments indicate that both adducts are well suited for the deposition of europium-containing films. In particular, the diglyme adduct has been successfully applied to Eu−O−F film deposition. A typical X-ray glancing incidence diffraction (GID) pattern of an Eu−O−F film deposited at 700 °C on quartz substrate is shown in Figure 7. Reflections point to the formation of two different polycrystalline oxyfluoride phases, the orthorhombic $Eu_6O_5F_8$ [38] and the rhombohedral EuOF.[39] The observed intensities are different from those reported for a polycrystalline powder, thus suggesting that some texturing occurs upon growth. An SEM micrograph of an Eu−O−F film deposited at 700 °C is reported in Figure 8. The image shows a very homogeneous surface with ≈1 μm diameter grains uniformly distributed.

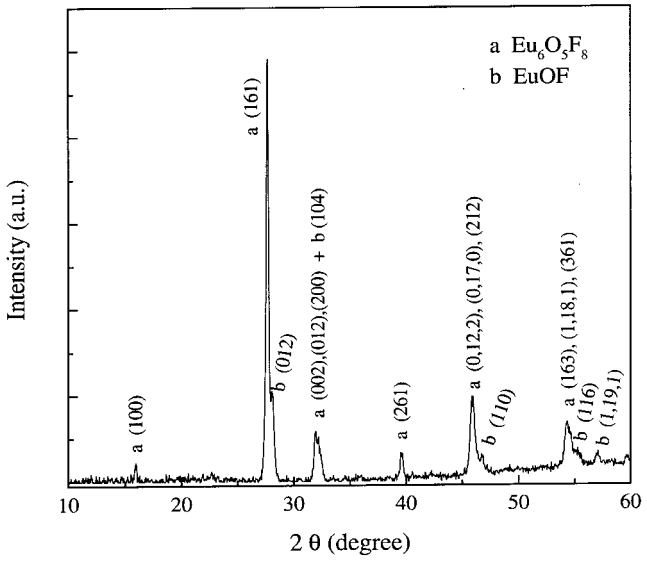

Figure 7. X-ray GID pattern of an MOCVD grown Eu−O−F film on a quartz substrate using the $Eu(hfa)_3$·diglyme precursor

Conclusions

The optical spectroscopy of the two $Eu(hfa)_3$·monoglyme and $Eu(hfa)_3$·diglyme adducts has been studied. The experimental results have provided information on the distortion of the coordination sphere around the lanthanide ion, on the covalence of the metal-ligand bond and on the coupling between electronic transitions and vibrational modes involving the europium(III) ion. Luminescence spectroscopy data have also been used to complement the DSC data of $Eu(hfa)_3$·diglyme in order to understand the nature of the phase transition at 71.4 °C.

There is evidence that the present $Eu(hfa)_3$·monoglyme and $Eu(hfa)_3$·diglyme adducts are thermally stable, highly volatile compounds that can be used even in atmospheric-pressure MOCVD deposition at temperatures lower than 200 °C. Low melting points allow their use as thermally stable precursors in the liquid phase, hence under constant vaporization and mass transport rates. Finally, both adducts **1** and **2**, analogously to the $La(hfa)_3$·diglyme precursor,[16] could act as liquid solvents for a large variety of metal precursors of relevance for MOCVD applicability, thus providing liquid multi-element single-sources for simultaneous delivery of different metal components in the required stoichiometries.

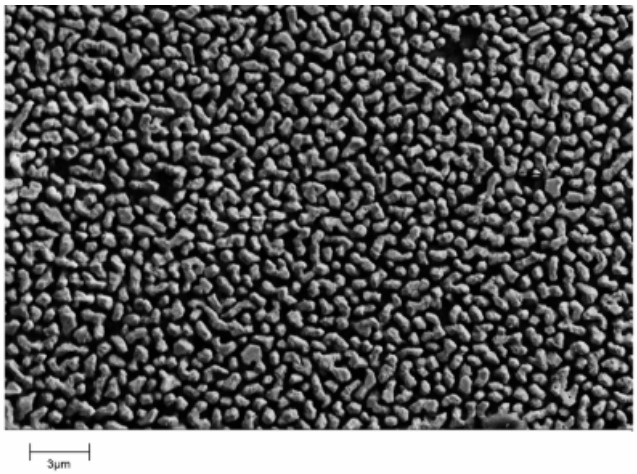

Figure 8. SEM micrograph of an MOCVD grown Eu−O−F film on a quartz substrate using the $Eu(hfa)_3$·diglyme precursor

Their vapor-phase transport characteristics at low- and atmospheric pressure make them attractive candidates not only for laboratory MOCVD processes but also for industrial applications.

Experimental Section

Reagents: Commercial Eu_2O_3, Hhfa, monoglyme, and diglyme (Aldrich) were used without any further purification.

General Procedures: Elemental microanalyses were performed in the Analytical Laboratories of the University of Catania. Infrared data were collected on a 684 Perkin−Elmer spectrometer either as nujol or hexachlorobutadiene mulls between KBr plates. Thermal measurements were made using a Mettler 3000 system equipped with a TG 50 thermobalance, a TC 10 processor and DSC 30 calorimeter. Weights of the samples were between 15−20 mg (TGA) and 4−10 mg (DSC). Analyses were made under prepurified nitrogen using a 5 °C/min heating rate. FAB mass spectra were obtained with a Kratos MS 50 spectrometer. The 488.0 nm line of a Spectra-Physics 2017 Argon laser was used to excite room temperature luminescence and Raman spectra. A fiber optic probe coupled to a Dilor Superhead, equipped with a suitable notch filter, was employed. The scattered signal was analyzed by a Jobin-Yvon HR460 monochromator and a Spectrum One CCD detector. A 1200 lines/mm grating was used to collect Raman and high resolution (≈2 cm^{-1}) luminescence spectra in the region of the $^5D_0 \rightarrow {}^7F_0$ transition of europium(III), whilst the other laser-excited luminescence spectra were measured using a 150 lines/mm grating. Low resolution emission and excitation spectra in the visible and UV regions were measured in the temperature range 20−90 °C using a JASCO FP-

777 spectrofluorimeter (bandwidths of 1.5 nm for both excitation and emission) and a conventional circulation thermostat. The decay curves of the luminescence were measured at room temperature using a Perkin−Elmer LS50 pulsed lamp spectrofluorimeter.

Synthesis of $Eu(hfa)_3$·monoglyme (1): The adduct was synthesized adopting a synthetic strategy analogous to that previously reported for the Gd analogue.[7] Eu_2O_3 (2.035 g, 5.78 mmol) was first suspended in hexane (200 mL) and then monoglyme (1.040 g, 11.56 mmol) was added to the suspension. Hhfa (7.217 g, 34.69 mmol) was added under vigorous stirring after 10 min. and the mixture was refluxed under stirring for 1 hour. The excess of europium oxide was then filtered off. Pale yellow crystals precipitated after partial evaporation of the solvent. The crystals were collected by filtration and dried under vacuum. The yield was 8.589 g (86%). The melting point of the crude product was 80−84 °C. − $C_{19}H_{13}EuF_{18}O_8$ (863.23): calcd. C 26.41, H 1.52; found C 26.52, H 1.47. The adduct quantitatively sublimes at 75−80 °C/10^{-3} Torr. − IR (nujol or hexachlorobutadiene): $\tilde{\nu}$ = 3620 (w), 3540 (w), 2930 (vs), 1660 (vs), 1610 (w), 1570 (m), 1540 (m), 1495 (s), 1455 (s), 1380 (m), 1350 (vw), 1260 (s), 1200 (s), 1150 (s), 1100 (m), 1060 (s), 1030 (w), 1010 (vw), 950 (w), 860 (m), 805 (m), 770 (w), 740 (w), 660 (s) cm^{-1}. The MS and IR data of the raw[40] and sublimed adduct are identical.

Synthesis of $Eu(hfa)_3$·diglyme (2): Prepared as described for the monoglyme adduct from Eu_2O_3 (1.956 g, 5.56 mmol), Hhfa (6.939 g, 33.36 mmol) and diglyme (1.489 g, 11.11 mmol). Yield 9.180 g (91%). The "apparent" melting point of the crude product was 72−74 °C (vide infra the DSC data). − $C_{21}H_{17}EuF_{18}O_9$ (907.28): calcd. C 27.77, H 1.89; found C 27.94, H 1.92. The adduct quantitatively sublimes at 85−90 °C/10^{-3} Torr. − IR (nujol or hexachlorobutadiene): $\tilde{\nu}$ = 2930 (s), 1650 (vs), 1605 (w), 1555 (m), 1530 (m), 1495 (s), 1460 (s), 1380 (m), 1350 (w), 1260 (s), 1205 (s), 1140 (s), 1090 (s), 1065 (m), 1045 (s), 1010 (m), 945 (m), 870 (m), 835 (vw), 800 (m), 770 (w), 740 (m), 650 (s) cm^{-1}. The MS and IR data of the raw and sublimed adduct are identical.

MOCVD Experiments: Low-pressure MOCVD depositions of Eu−O−F films were carried out under O_2 (500 sccm) flow as carrier and reaction gas, using a horizontal hot-wall reactor. The $Eu(hfa)_3$·diglyme source temperature was maintained at 120 °C. Quartz slides were used as substrates in the 600−700 °C temperature range. Scanning Electron Microscopy (SEM) micrographs were recorded using a LEO IRIDIUM 1450 Electron Microscope. X-ray glancing incidence diffraction (GID) patterns were recorded on a Bruker-AXS D5005 θ-θ X-ray diffractometer equipped with a Goebel mirror and a thin film attachment using Cu-K_α radiation operating at 40KV/ 30 mA.

Acknowledgments

The authors gratefully thank Erica Viviani (Università di Verona) for expert technical assistance. The Ministero dell'Università e della Ricerca Scientifica e Tecnologica (MURST, Rome) is also gratefully acknowledged for financial support within P.R.I.N. programs.

[1] S. R. Drake, A. Lyons, D. J. Otway, A. M. Z. Slawin, D. J. Williams, *J. Chem. Soc., Dalton Trans.* **1993**, 2379−2386.
[2] S. R. Drake, M. B. Hursthouse, K. M. A. Malik, S. A. S. Miller, D. J. Otway, *Inorg. Chem.* **1993**, *32*, 4464−4471.
[3] D. C. Bradley, H. Chudzynska, M. B. Hursthouse, M. Motevalli, *Polyhedron* **1994**, *13*, 7−14.
[4] I. Baxter, S. R. Drake, M. B. Hursthouse, K. M. A. Malik, J. MacAleese, D. J. Otway, J. C. Plakatouras, *Inorg. Chem.* **1995**, *34*, 1384−1394.
[5] R. Amano, Y. Shiokawa, N. Sato, Y. Suzuki, *J. Radioanal. Nucl. Chem.* **1993**, *172*, 81−86.
[6] G. Malandrino, R. Licata, F. Castelli, I. L. Fragalà,, C. Benelli, *Inorg. Chem.* **1995**, *34*, 6233−6234.
[7] G. Malandrino, O. Incontro, F. Castelli, I. L. Fragalà, C. Benelli, *Chem. Mater.* **1996**, *8*, 1292−1297.
[8] G. Malandrino, C. Benelli, F. Castelli, I. L. Fragalà, *Chem. Mater.* **1998**, *10*, 3434−3444.
[9] G. Malandrino, I. L. Fragalà, S. Aime, W. Dastrù, R. Gobetto, C. Benelli, *J. Chem. Soc., Dalton Trans.* **1998**, 1509−1512.
[10] K. D. Pollard, J. J. Vittal, G. P. A. Yap, R. J. Puddephatt, *J. Chem. Soc., Dalton Trans.* **1998**, 1265−1267.
[11] J. H. Lee, Y. S. Jung, Y. S. Sohn, S. J. Kang, *Bull. Kor. Chem. Soc.* **1998**, *19*, 231−235.
[12] S. J. Kang, Y. S. Jung, I. H. Suh, *Bull. Kor. Chem. Soc.* **1999**, *20*, 95−98.
[13] K. D. Pollard, H. A. Jenkins,, R. J. Puddephatt, *Chem. Mater.* **2000**, *12*, 701−710.
[14] G. Malandrino, R. Lo Nigro, C. Benelli, F. Castelli, I. L. Fragalà, *Chem. Vap. Depos.* **2000**, *6*, 233−238.
[15] G. Malandrino, A. Frassica, I. L. Fragalà, *Chem. Vap. Depos.* **1997**, *3*, 306−309.
[16] G. Malandrino, I. L. Fragalà, P. Scardi, *Chem. Mater.* **1998**, *10*, 3765−3768.
[17] G. Malandrino, I. L. Fragalà, *Electrochemical Society Proceedings*, **1997**, Vol. *97−25*, 844−851
[18] *Chemical Vapor Deposition: Principles and Applications* (Eds.: M. L. Hitchman, K. F. Jensen , Academic Press, London, **1993**.
[19] H. Sato, *Jpn. J. Appl. Phys.* **1994**, *33*, L371−L373.
[20] S. J. Kang, Y. S. Jung, Y. S. Sohn, *Bull. Kor. Chem. Soc.* **1997**, *18*, 75−80.
[21] G. Blasse, B. C. Grabmaier, *Luminescent Materials*, Springer Verlag, Berlin, **1994**.
[22] D. Lin-Vien, N. B. Colthup, W. G. Fateley, J. G. Grasselli, *The Handbook of Infrared and Raman Characteristic Frequencies of Organic Molecules*, Academic Press, San Diego, CA, **1991**.
[23] I. K. Igumenov, P. P. Semyannikov, S. V. Belaya, A. S. Zanina, S. I. Shergina, I. E. Sokolov, *Polyhedron* **1996**, *15*, 4521−4530.
[24] M. Wachtler, A. Speghini, K. Gatterer, H. P. Fritzer, D. Ajò, M. Bettinelli, *J. Amer. Ceram. Soc.* **1998**, *81*, 2045−2052.
[25] D. Braga, *Chem. Rev.* **1992**, *92*, 633−665.
[26] G. Malandrino, F. Castelli, I. L. Fragalà, *Inorg. Chim. Acta* **1994**, *224*, 203−207.
[27] J. A. Capobianco, P. P. Proulx, N. Raspa, *Chem. Phys. Lett.* **1989**, *161*, 151−157.
[28] P. Caro, O. Beaury, E. Antic, *J. Phys.* **1976**, *37*, 671−676.
[29] E. W. J. L. Oomen, A. M. A. van Dongen, *J. Non-Cryst. Solids* **1989**, *111*, 205−213.
[30] G. Blasse, *Structure and Bonding (Berlin)* **1976**, *26*, 43−79.
[31] *Vibronic Processes in Inorganic Chemistry* (Ed.: C. D. Flint), Kluwer, Dordrecht, **1989**.
[32] G. Blasse, *Int. Rev. Phys. Chem.* **1992**, *11*, 71−100.
[33] G. Blasse, *Inorg. Chim. Acta* **1990**, *167*, 33−37.
[34] M. Wachtler, A. Speghini, S. Pigorini, R. Rolli, M. Bettinelli, *J. Non-Cryst. Solids* **1997**, *217*, 111−114.
[35] *Lanthanide Probes in Life, Chemical and Earth Sciences, Theory and Practice* (Eds.: J.-C. G. Bünzli, G. R. Choppin), Elsevier, Amsterdam, **1989**, p. 219−293.
[36] S. Todoroki, K. Hirao, N. Soga, *J. Alloys Compd.* **1993**, *193*, 207−209.
[37] Although the X-ray crystal structure of **2** has been reported,[20] this value is not available and, therefore, the M−M distance in the Gd isostructural compound has been considered.
[38] ICDD No. 26−637.
[39] ICDD No. 26−636.
[40] Used without any further purification.

Received August 12, 2000
[I00304]